SURFACE AND INTERFACE ANALYSIS
Surf. Interface Anal. 2005; **37**: 809–820
Published online 2 September 2005 in Wiley InterScience (www.interscience.wiley.com). DOI: 10.1002/sia.2081

SIA

Quantitative AES, XPS and RBS determination of intergranular bismuth coverage in copper bicrystals at 500 °C

V. Laporte,[1,2]* P. Berger[3] and K. Wolski[1]

[1] Centre Science des Matériaux et des Structures, Ecole Nationale Supérieure des Mines de Saint-Etienne, CNRS PECM UMR 5146, 158, cours Fauriel, F-42023 Saint-Etienne cedex 02, France
[2] Ecole Polytechnique Fédérale de Lausanne (EPFL), Laboratoire de Métallurgie Mécanique, Station 12, CH-1015 Lausanne, Switzerland
[3] Laboratoire Pierre SÜE (CEA/CNRS), UMR9956 CEA/SACLAY, F-91191 Gif Sur Yvette Cedex, France

Received 16 December 2004; Revised 30 June 2005; Accepted 13 July 2005

We report on a comparative measurement of intergranular bismuth coverage on a copper substrate using Auger electron spectroscopy (AES), x-ray photoelectron spectroscopy (XPS) and Rutherford backscattering spectroscopy (RBS). Bicrystalline copper samples were put in presence of bismuth vapour at 500 °C (consequently embrittled by the grain-boundary penetration of Bi atoms), water-quenched and subsequently fractured at room temperature. Each fracture surface was analysed by AES, XPS and RBS with the help of quantitative procedures developed for each of the three techniques. All possible sources of discrepancy were carefully examined. The combined quantitative approaches have led to excellent agreement. Such a good agreement constitutes a necessary condition to begin a critical discussion on the mechanisms potentially involved in the liquid metal embrittlement (LME) phenomenon. Copyright © 2005 John Wiley & Sons, Ltd.

KEYWORDS: liquid metal embrittlement; intergranular penetration; AES; XPS; RBS

INTRODUCTION

Intergranular brittleness of metallic materials is known to be the result of either impurity segregation from the bulk material or intergranular diffusion of embrittling species from an aggressive external environment. When such an environment is constituted by liquid lead–bismuth used in spallation target of hybrid systems,[1–3] it can result notably in the liquid metal embrittlement (LME) phenomenon.

In spite of a number of proposed mechanisms reviewed in many articles,[4,5] there is still a lack of understanding, especially, in the prediction of LME. In order to determine the mechanism controlling this phenomenon, the absolute amount of heavy metal in the grain boundaries must be known with precision. In fact, if this quantity is in the range one or two monolayers, intergranular diffusion, until equilibrium segregation, could be responsible for the observed embrittlement. Otherwise (thickness $\gg$ 2 monolayers), it would appear inevitable to introduce a grain-boundary wetting formalism, where grain boundaries can be replaced by liquid phases after being penetrated by foreign atoms. Hence, the precise determination of the thickness can actually give valuable information about elementary mechanisms involved in the embrittlement.

*Correspondence to: V. Laporte, Ecole Polytechnique Fédérale de Lausanne (EPFL), Laboratoire de Métallurgie Mécanique, Station 12, CH-1015 Lausanne, Switzerland. E-mail: vincent.laporte@epfl.ch

This is the reason why we decided to use three independent methods: Auger electron spectroscopy (AES), x-ray photoelectron spectroscopy (XPS) and Rutherford backscattering spectroscopy (RBS), all of them known for their ability to produce quantitative results. We have chosen to study this phenomenon using a model system known for its LME predisposition:[6] solid copper in contact with liquid bismuth. One of the main interests of this system is that copper grain boundaries remain brittle at room temperature if they have been previously exposed to bismuth,[7] and this brittleness allows first AES and XPS analyses after *in situ* fractures, and second RBS analyses, all of them on the same specimen and the same fracture surface.

This kind of study has been already done for another similar system: solid nickel in contact with liquid bismuth, where bismuth has an even stronger intergranular embrittling effect. The authors[8,9] established that polycrystalline nickel was embrittled by a nanometer-thick intergranular film of a bismuth-rich alloy after heat treatment at 700 °C where nickel, either directly or through its vapour was in contact with oversaturated bismuth. This work also suggests the use of vapour contact instead of direct contact to observe bismuth embrittlement of copper.

The purpose of the present paper is to quantify the amount of bismuth present in copper grain boundaries using independent AES, XPS and RBS measurements made on the same fracture surfaces of bicrystalline copper specimens embrittled by contact with liquid bismuth. These results

will be shortly discussed with respect to potentially efficient mechanisms of LME.

EXPERIMENTAL

The copper bicrystal used in this study had a 50° ⟨100⟩ tilt grain boundary. It was prepared by melting and controlled solidification in a horizontal furnace (using a bicrystalline seed on an alumina mould) and cut by spark erosion to get parallelepipeds (1.5 × 1.5 × 20 mm) with the grain boundary at approximately half the distance along the length. It was then chemically polished in order to remove residual stresses introduced by spark erosion (thus avoiding any recrystallisation during the subsequent heat treatment).

Each copper specimen and a few pieces of pure solid bismuth were placed in a silica tube sealed under argon, in such a way that no direct contact between the two metals was possible during the heat treatment (Fig. 1). This procedure had a twofold advantage: (i) it avoided copper dissolution into liquid bismuth, the rate of which can reach several tens of microns per hour[10] and (ii) it limited the quantity of bismuth introduced in the AES–XPS main chamber, thereby limiting possible bismuth evaporation problems during external heat-maintenance operations.

All heat treatments were performed at 500 °C (>271 °C, which is the melting point of bismuth) and two time periods were selected in order to get a complete and homogeneous penetration of a unique grain boundary: 48 h (samples S048-1 and S048-2) and 137 h (samples S137-1 and S137-2). AES analyses were performed for all specimens, XPS analyses were achieved only for S048-1 and S048-2 and RBS analyses for S048-1 and S137-1.

At 500 °C, the total pressure of bismuth vapour is about 4×10^{-8} bar, and this value allows the deposition of several nanometers of bismuth on the external surfaces of the bicrystal specimen as revealed by glow discharge optical spectroscopy. During the heat treatment, this liquid layer can act as a source for the bismuth grain boundary penetration into copper. This procedure has been suggested by the previous work of Fraczkiewicz at the Ecole des Mines de Saint-Etienne on the study of the intergranular segregation of bismuth in copper bicristals,[11,12] also applied by Marié of the same laboratory to study the intergranular penetration of bismuth into nickel bicristals and polycrystals[8,13] and, probably, independently developed by Chang in his recent thesis on the intergranular segregation of bismuth in copper polycrystals.[14] Such a procedure was thus shown to be equivalent to the direct contact between copper and bismuth-rich Bi–Cu alloy.[15] After the heat treatment, specimens were water-quenched in a few seconds.

In order to reveal the grain boundary composition, the specimens were broken by bending (for S048-1 and S048-2) or by tensile test (for S137-1 and S137-2) within the main chamber of the AES–XPS spectrometer. The fracture surfaces were always intergranular and completely brittle, leading to homogeneously flat surfaces. Only one side of each specimen could be analysed after *in situ* fracture by AES and XPS (Fig. 2), but it is worth noticing that both were analysed by RBS in order to confirm the assumption of equirepartition of bismuth on both sides.

A vacuum of less than 5×10^{-10} mbar in the main chamber together with the low reactivity of fracture surfaces allowed an 8-h long series of AES and XPS measurements without any noticeable carbon or oxygen contamination. RBS analyses were performed six months later in the Pierre Süe Laboratory of the French Atomic Energy Commission (CEA). A detailed description of the quantification procedures used for each technique is presented here and, in the following, we will use τ_{AES}, τ_{XPS} and τ_{RBS} to refer to the amount of bismuth (expressed as fraction of monolayer) determined using the corresponding techniques. These values correspond to the amount of bismuth on one fracture surface; therefore, the total amount of bismuth in the grain boundary is the double, i.e. $2 \times \tau$.

AES quantification

AES analyses were performed under a 5-keV primary electron beam incident at an angle of $\varphi = 50°$ with respect to the surface normal. AES spectra were recorded with a Cameca Mac III analyser. The emitted electrons were collected at a resolution of 1 eV with a step of 0.25 eV and at an angle of $\theta = 20°$ with respect to the surface normal. The AES-analysed areas were either about 50 μm^2 spots or several hundreds of μm^2 scans, made on different places of the fracture surface in order to evaluate the homogeneity of the bismuth coverage.

AES intensities expression

Assuming that bismuth is present as a fraction of monolayer τ_{AES} and using a discrete summation (monolayer by monolayer), the AES bismuth and copper intensities can be expressed as:

$$I_{Bi}^{AES} = \tau_{AES} K_{AES} \beta_{Bi} n_{Bi} R_{Bi}^{Cu} \quad (1)$$

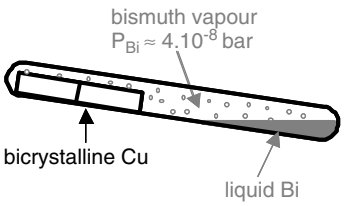

Figure 1. Experimental procedure: bicrystalline Cu and pure Bi are placed in a silica tube sealed under argon so that no direct contact is possible during heat treatment in the furnace at 500 °C.

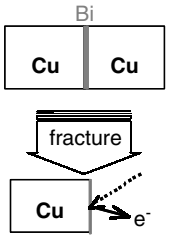

Figure 2. *In situ* fracture of the embrittled bicrystals: coupled XPS–AES measurements could be performed on only one of the sides of the fracture surface.

and

$$I_{Cu}^{AES} = K_{AES}\beta_{Cu}n_{Cu}R_{Cu}^{Cu}\left[\tau_{AES}k_p^{Bi}k_{Cu}^{Bi} + (1-\tau_{AES})\right]\sum_{i=0}^{+\infty}\left(k_p^{Cu}k_{Cu}^{Cu}\right)^i$$

$$= K_{AES}\beta_{Cu}n_{Cu}R_{Cu}^{Cu}\left[\frac{\tau_{AES}k_p^{Bi}k_{Cu}^{Bi} + (1-\tau_{AES})}{1-k_p^{Cu}k_{Cu}^{Cu}}\right] \quad (2)$$

with:

K_{AES} depending on instrumental factors and analysis conditions (K_{AES} is the same for all elements during the analysis of a given specimen),

β_A depending on the chosen auger transition for the element A,

n_A the numbers of A atoms per unit area,

R_A^M the backscattering factor for a chosen transition of the element A through the matrix M,

$k_p^M = \exp\left(\frac{-d_M}{\lambda_p^M\cos\varphi}\right)$ the attenuation factor of primary electrons through the matrix M,

$k_A^M = \exp\left(\frac{-d_M}{\lambda_A^M\cos\theta}\right)$ the attenuation factor of an electron of A in the matrix M,

d_M the monolayer thickness of the matrix M and

λ_A^M the inelastic mean free path for an electron of A in the matrix M (λ_p^M meaning the inelastic mean free path of the primary electrons through the matrix M) [the choice of this parameter instead of the effective attenuation length is addressed in the discussion].

Difficulties in AES quantifications lie essentially in β determination that involves the evaluation of the ionisation cross-section, the deexcitation probability and the analyser transmission function. Pure elements (both copper and bismuth) were therefore used to evaluate the ratio $\frac{\beta_{Bi}}{\beta_{Cu}}$. For pure elements analysed under the same experimental conditions (electron beam and geometrical considerations), the following equations can be written:

$$I_{Bi}^0 = K_A^0\beta_{Bi}n_{Bi}R_{Bi}^{Bi}\sum_{i=0}^{+\infty}\left(k_p^{Bi}k_{Bi}^{Bi}\right)^i$$

$$= \frac{K_A^0\beta_{Bi}n_{Bi}R_{Bi}^{Bi}}{1-k_p^{Bi}k_{Bi}^{Bi}} \quad (3)$$

and

$$I_{Cu}^0 = K_A^0\beta_{Cu}n_{Cu}R_{Cu}^{Cu}\sum_{i=0}^{+\infty}\left(k_p^{Cu}k_{Cu}^{Cu}\right)^i$$

$$= \frac{K_A^0\beta_{Cu}n_{Cu}R_{Cu}^{Cu}}{1-k_p^{Cu}k_{Cu}^{Cu}} \quad (4)$$

which leads to:

$$\frac{\beta_{Bi}}{\beta_{Cu}} = \frac{I_{Bi}^0 n_{Cu}R_{Cu}^{Cu}}{I_{Cu}^0 n_{Bi}R_{Bi}^{Bi}}\frac{1-k_p^{Bi}k_{Bi}^{Bi}}{1-k_p^{Cu}k_{Cu}^{Cu}} \quad (5)$$

and thus:

$$\frac{I_{Bi}^{AES}}{I_{Cu}^{AES}} = \frac{I_{Bi}^0}{I_{Cu}^0}\times\frac{R_{Bi}^{Cu}}{R_{Bi}^{Bi}}\times\frac{1-k_p^{Bi}k_{Bi}^{Bi}}{\frac{(1-\tau_{AES})}{\tau_{AES}}+k_p^{Bi}k_{Cu}^{Bi}} \quad (6)$$

It is worth noticing here that the same relationship can be obtained using a continuous summation (see appendix for details).

AES parameters evaluation

The backscattering factors R were obtained using the empirical formula:[16]

$$R_A^M = 1 + (2.34 - 2.10Z_M^{0.14})\times\left(\frac{E_p}{E_L^A}\right)^{-0.35} + (2.58Z_M^{0.14} - 2.98). \quad (7)$$

With $Z_{Cu} = 29$, $Z_{Bi} = 83$, $E_p = 5000$ eV and $E_L = 161.9$ eV (for the bismuth $N_6O_{45}O_{45}$ transition at 101 eV), $R_{Bi}^{Cu} \approx 1.85$, $R_{Bi}^{Bi} \approx 2.34$ and finally $\frac{R_{Bi}^{Cu}}{R_{Bi}^{Bi}} \approx 0.8$.

The bismuth monolayer thickness d_{Bi} was evaluated as the cubic root of the atomic volume:

$$d_{Bi} \approx \sqrt[3]{\frac{M_{Bi}}{N_{avo}\rho_{Bi}}}. \quad (8)$$

With $M_{Bi} \approx 208.98$ g mol^{-1} the molar mass, N_{avo}, the number of atoms per mole and $\rho_{Bi} \approx 9.8$ g cm^{-3} the density, that leads to $d_{Bi} \approx 0.329$ nm.

The inelastic mean free paths (IMFP) λ_A^M were determined using the semiempirical formula:[17–19]

$$\lambda_A^M = \frac{E_c^A}{(E_p^M)^2\times\left[B_M\times\ln(\gamma_M E_c^A) - \frac{C}{E_c^A} + \frac{D}{(E_c^A)^2}\right]} \quad (9)$$

with λ_A^M expressed in angstroms and E_c (kinetic energy) in electronvolts and:

$$E_p^M = 28.8\times\sqrt{\frac{N_v^M\times\rho_M}{\mathrm{M}_M}} \quad (10)$$

(N_V: number of valence electrons, ρ: density and M: molar mass)

$$B_M = -0.1 + \frac{0.944}{E_p^M} + 0.069(\rho_M)^{0.1} \quad (11)$$

$$\gamma_M = 0.191(\rho_M)^{-0.5} \quad (12)$$

$$C_M = 1.97 - 0.91\times U_M \quad (13)$$

$$D_M = 53.4 - 20.8\times U_M \quad (14)$$

$$U_M = \frac{(E_p^M)^2}{829.4} \quad (15)$$

The transitions used in the analyses were the Cu $M_{23}VV$ (kinetic energy: 59 eV) and the Bi $N_6O_{45}O_{45}$ (kinetic energy: 101 eV). The IMFP were then calculated:

$\lambda_p^{Bi} \approx 8.274$ nm (≈25.2 monolayers of bismuth)

$\lambda_{Bi}^{Bi} \approx 0.602$ nm (≈1.8 monolayers of bismuth)

$\lambda_{Cu}^{Bi} \approx 0.564$ nm (≈1.7 monolayers of bismuth)

Then, Eqn (6) becomes:

$$\tau_{AES} = \frac{\frac{I_{Bi}^{AES}}{I_{Cu}^{AES}}}{0.49\times\frac{I_{Bi}^{AES}}{I_{Cu}^{AES}} + 0.38\times\frac{I_{Bi}^0}{I_{Cu}^0}} \quad (16)$$

AES results

Experimental intensities were determined using peak-to-peak heights evaluated after differentiation of the smoothed direct spectra (Fig. 3). With such a procedure, the experimental standard intensity ratio $\frac{I^0_{Bi}}{I^0_{Cu}}$ measured on pure elements was found to be about 1: $\frac{I^0_{Bi}}{I^0_{Cu}} \approx 1 \pm 0.1$. The fraction of bismuth monolayer τ_{AES} present on the fracture surface is then related to the experimental bismuth-to-copper intensity ratio with the following equation:

$$\tau_{AES} \approx \frac{\frac{I^{AES}_{Bi}}{I^{AES}_{Cu}}}{0.49 \times \frac{I^{AES}_{Bi}}{I^{AES}_{Cu}} + 0.38} \tag{17}$$

Experimental bismuth-to-copper AES intensity ratios and corresponding fractions of the bismuth monolayer are presented in Table 1.

In addition to the discrepancies introduced by the dispersion of experimental results, those due to the quantification parameter evaluation are to be discussed: namely, the IMFP evaluation, the experimental standard intensity ratio $\frac{I^0_{Bi}}{I^0_{Cu}}$ evaluation and the primary electron beam attenuation can modify Eqn (17). First, the IMFP can be evaluated using another empirical equation[20] different from that proposed in the previous section:

$$\lambda^M_A = 538(E^A_c)^{-2} + 0.41\sqrt{d_M E^A_c} \tag{18}$$

With such a relationship, the IMFP become:

$\lambda^{Bi}_p \approx 5.471$ nm ($\approx$16.6 monolayers of bismuth)

$\lambda^{Bi}_{Bi} \approx 0.795$ nm ($\approx$2.4 monolayers of bismuth)

$\lambda^{Bi}_{Cu} \approx 0.645$ nm ($\approx$2.0 monolayers of bismuth)

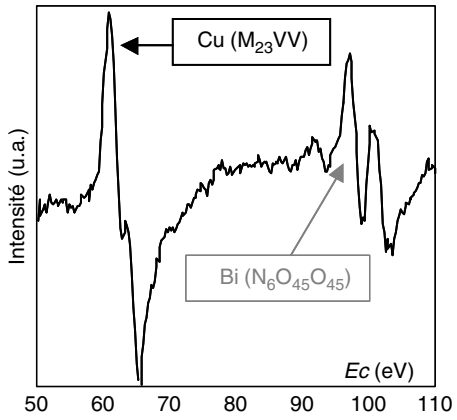

Figure 3. Example of a differential AES spectrum obtained for S048-1 (*in situ* fractured Cu 48 h-specimen).

As a result, Eqn (17) changes into Eqn (19) and produces a maximum deviation from our first τ_{AES} calculation of less than +0.08 (Fig. 4).

$$\tau_{AES} \approx \frac{\frac{I^{AES}_{Bi}}{I^{AES}_{Cu}}}{0.48 \times \frac{I^{AES}_{Bi}}{I^{AES}_{Cu}} + 0.33} \tag{19}$$

Second, the discrepancy of the experimental $\frac{I^0_{Bi}}{I^0_{Cu}}$ ratio induces a maximum deviation from our τ_{AES} calculation of less than $\pm$0.05 (Fig. 5). Lastly, the primary electron beam attenuation is usually neglected in AES quantification, but it is kept under consideration in our study. The first reason is that the intensity expressions are more rigorous and general. The second lies in the numerical values obtained for this attenuation, which can reach significant level:

$\exp\left(\frac{-d_{Bi}}{\lambda^{Bi}_p \cos\varphi}\right) \approx 0.94$ if we use the first semiempirical expression presented for the inelastic mean free path[17,18] and

$\exp\left(\frac{-d_{Bi}}{\lambda^{Bi}_p \cos\varphi}\right) \approx 0.91$ if we use the second one.[20]

On another hand, the other parameters do not introduce any significant variation in our results. For example, even if several relations exist for the backscattering factor evaluation,[16,21] the evaluation of the ratio $\frac{R^{Cu}_{Bi}}{R^{Bi}_{Bi}}$ is not significantly altered by the use of these different relations.

Taking into account the above mentioned uncertainties allows us to conclude that bismuth monolayer fraction given by AES measurements is $\tau_{AES} = 82\% \pm 18\%$.

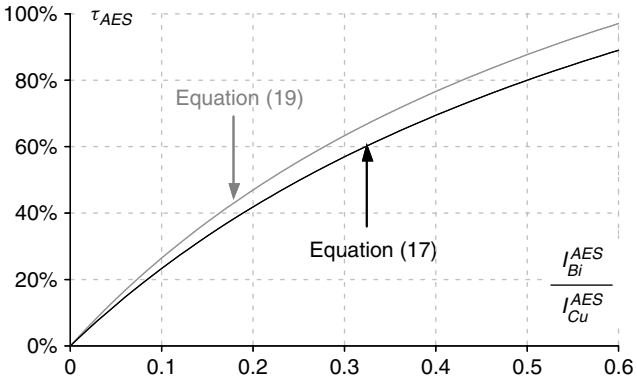

Figure 4. Graphical evolution of τ_{AES} as a function of $\frac{I^{AES}_{Bi}}{I^{AES}_{Cu}}$ depending on the empirical equation chosen for the inelastic mean free path evaluation: black curve is obtained with Eqn (17) and grey curve with Eqn (19).

Table 1. Experimental bismuth-to-copper AES intensity ratios (obtained using peak-to-peak evaluation after differentiation of the smoothed direct AES spectra) and their corresponding fractions of bismuth monolayer τ_{AES} obtained using Eqn (17): indicated discrepancies are only those introduced by the dispersion of results

	S048-1	S048-2	S137-1	S137-2
$\frac{I^{AES}_{Bi}}{I^{AES}_{Cu}}$	0.51 ± 0.02 (10 analyses)	0.50 ± 0.02 (4 analyses)	0.60 ± 0.02 (5 analyses)	0.43 ± 0.03 (4 analyses)
τ_{AES}	0.81 ± 0.04	0.80 ± 0.06	0.89 ± 0.06	0.73 ± 0.08

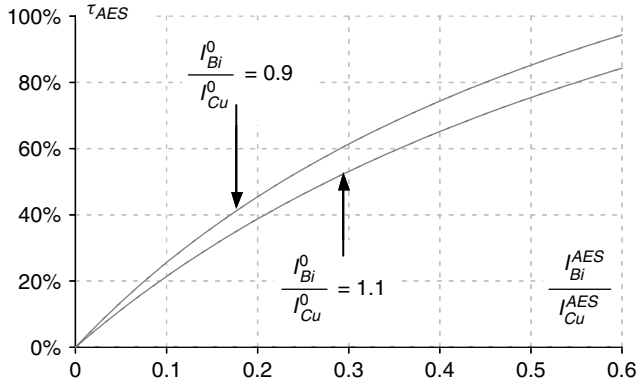

Figure 5. Graphical evolution of τ_{AES} as a function of $\frac{I^{AES}_{Bi}}{I^{AES}_{Cu}}$ representing the discrepancy due to the experimental evaluation of $\frac{I^0_{Bi}}{I^0_{Cu}}$ ratio: both curves are obtained using Eqn (16).

XPS quantification

After the *in situ* fracture of the specimens, one each of S048-1 and S048-2 fracture surfaces were excited with Mg Kα X-rays incident at an angle of 72° with respect to the surface normal. X-ray-excited photoelectron spectra were recorded with a Cameca Mac III analyser. The emitted electrons were collected with a 1-eV energy resolution at an angle of $\theta = 20°$ with respect to the surface normal. Due to the high spot size of photons from the twin anode source, XPS spot size is greater than the *in situ* opened fracture surface of $1.5 \times 1.5\ mm^2$. A specific procedure was hence used on both S048-1 and S048-2 before *in situ* fracture, consisting of gold deposition on their external surfaces in order to suppress any possible contribution of the bismuth-covered lateral surfaces after *in situ* fracture.

XPS discrete summation

Assuming again that bismuth is present on copper as a homogeneous fraction of monolayer τ_{XPS} and using a discrete summation, the XPS bismuth and copper intensities can be expressed as:

$$I^{XPS}_{Bi} = \tau_{XPS} K_{XPS} n_{Bi} \sigma_{Bi} T_{Bi} \tag{20}$$

and

$$I^{XPS}_{Cu} = K_{XPS} n_{Cu} \sigma_{Cu} T_{Cu} [(1 - \tau_{XPS}) + \tau_{XPS} k^{Bi}_{Cu}] \sum_{i=0}^{+\infty} (k^{Cu}_{Cu})^i$$

$$= K_{XPS} n_{Cu} \sigma_{Cu} T_{Cu} \frac{[(1 - \tau_{XPS}) + \tau_{XPS} k^{Bi}_{Cu}]}{1 - k^{Cu}_{Cu}} \tag{21}$$

with:

- K_{XPS} depending on instrumental factors and analysis conditions (K_{XPS} is the same for all elements during the analysis of a given specimen),
- σ_A the photoionisation cross-section,
- T_A the transmission function,
- d_{Bi} the bismuth monolayer thickness and
- λ^M_A the inelastic mean free path for an electron of A in the matrix M.

These expressions lead to:

$$\tau_{XPS} = \frac{\frac{I^{XPS}_{Bi}}{I^{XPS}_{Cu}}}{\frac{n_{Bi}\sigma_{Bi}T_{Bi}}{n_{Cu}\sigma_{Cu}T_{Cu}}[1 - k^{Cu}_{Cu}] + \frac{I^{XPS}_{Bi}}{I^{XPS}_{Cu}}[1 - k^{Bi}_{Cu}]} \tag{22}$$

and, with the chosen transitions (Cu-2p$^{3/2}$ single peak with a kinetic energy of 319.6 eV and Bi-4f$^{5/2}$ and Bi-4f$^{7/2}$ peaks with the respective kinetic energies of 1089.6 and 1094.6 eV), to:

$$\tau_{XPS} = \frac{\frac{I^{XPS}_{Bi}}{I^{XPS}_{Cu}}}{\frac{n_{Bi}[\sigma_{Bi-4f^{7/2}} + \sigma_{Bi-4f^{5/2}}]T_{Bi}}{n_{Cu}\sigma_{Cu-2p^{3/2}}T_{Cu}}[1 - k^{Cu}_{Cu}] + \frac{I^{XPS}_{Bi}}{I^{XPS}_{Cu}}.[1 - k^{Bi}_{Cu}]} \tag{23}$$

XPS parameters evaluation

Term n_A is estimated using the following relationship:

$$n_A = \frac{\rho_A N_{avo}}{M_A} \times d_A \tag{24}$$

With ρ_A being the density, N_{avo} the number of atoms per mole, M_A the molar mass and d_A the monolayer thickness, the followings values were obtained:

$n_{Bi} \approx 9.3$ atoms/nm^2 and $n_{Cu} \approx 19.2$ atoms/nm^2.

Scofield tabulation[22] was used to get the cross-section σ for the chosen transitions:

$$\sigma_{Cu-2p^{3/2}} = 15.87$$
$$\sigma_{Bi-4f^{7/2}} = 13.85$$
$$\sigma_{Bi-4f^{5/2}} = 10.93 \tag{25}$$

For λ^M_A, the same expression[17,18] was used as in AES parameters evaluation and led, for Cu-2p$^{3/2}$, to:

$\lambda^{Bi}_{Cu} \approx 1.051$ nm (≈3.2 Bi monolayers) and

$\lambda^{Cu}_{Cu} \approx 0.703$ nm (≈3.1 Cu monolayers).

Factor T depends only on the photoelectron kinetic energy. Rather than using an empirical equation describing this dependency, we have chosen to evaluate the T_{Bi}/T_{Cu} ratio using the pure copper spectrum obtained under the same analysis conditions on a reference sample and assuming that $T_{Bi-4f} \approx T_{Cu-3p}$. This assumption is supported by both the proximity of energy levels (1089.6 and 1094.6 eV for Bi-4f as compared with 1176.6 for Cu-3p) and the very limited evolution of T for high kinetic energies. For pure copper, intensities can be written as follows:

$$I^0_{Cu}(2p^{3/2}) = K^0 N_{Cu} \lambda^{Cu}_{Cu-2p^{3/2}} \sigma_{Cu-2p^{3/2}} T_{Cu-2p^{3/2}} \tag{26}$$

$$I^0_{Cu}(3p) = K^0 N_{Cu} \lambda^{Cu}_{Cu-3p} [\sigma_{Cu-3p^{1/2}} + \sigma_{Cu-3p^{3/2}}] T_{Cu-3p} \tag{27}$$

and therefore:

$$\frac{T_{Cu-3p}}{T_{Cu-2p^{3/2}}} = \frac{I^0_{Cu-3p}}{I^0_{Cu-2p^{3/2}}} \times \frac{\lambda^{Cu}_{Cu-2p^{3/2}}}{\lambda^{Cu}_{Cu-3p}} \times \frac{\sigma_{Cu-2p^{3/2}}}{[\sigma_{Cu-3p^{1/2}} + \sigma_{Cu-3p^{3/2}}]} \tag{28}$$

Using the same semiempirical equation[17,18] for the IMFP, and Scofield tabulation[22] for the photoionisation cross-section, the previous relationship becomes:

$$\frac{T_{Cu-3p}}{T_{Cu-2p^{3/2}}} = \frac{I^0_{Cu-3p}}{I^0_{Cu-2p^{3/2}}} \times 2.8 \tag{29}$$

Experimentally, we obtained: $\frac{I^0_{Cu-3p}}{I^0_{Cu-2p^{3/2}}} \approx 0.16$, leading to:

$$\left(\frac{T_{Bi-4f}}{T_{Cu-2p^{3/2}}} \approx\right) \frac{T_{Cu-3p}}{T_{Cu-2p^{3/2}}} \approx 0.44. \tag{30}$$

That is to be compared with the value 0.74 obtained with the help of an empirical relationship between T and E_c: $T = 2.5\exp(-0.23E_c) + 1.49 - 5.76 \times 10^{-4}E_c + 8.74 \times 10^{-8}E_c^2$, as provided by Cameca.

Using the previously described parameters calculation, the following relationship appears:

$$\tau_{XPS} \approx \frac{\frac{I^{XPS}_{Bi}}{I^{XPS}_{Cu}}}{0.10 + 0.28 \times \frac{I^{XPS}_{Bi}}{I^{XPS}_{Cu}}} \tag{31}$$

XPS results

Experimental intensities have been determined using area calculations with linear subtraction on direct spectra (Fig. 6). Experimental bismuth to copper intensity ratios and corresponding fractions of bismuth monolayer are presented in Table 2.

The only parameter evaluations that can add discrepancy to the results concern the IMFP. The same empirical equation[20] as proposed in AES discrepancy evaluation can be used and changes Eqn (31) into Eqn (32).

$$\tau_{XPS} \approx \frac{\frac{I^{XPS}_{Bi}}{I^{XPS}_{Cu}}}{0.08 + 0.22\frac{I^{XPS}_{Bi}}{I^{XPS}_{Cu}}} \tag{32}$$

Table 2. Experimental bismuth to copper XPS intensity ratios (obtained using area evaluation on the direct XPS spectra) and their corresponding fractions of bismuth monolayer τ_{XPS} obtained using Eqn (31) for discrete summation: indicated discrepancies are those introduced by the graphical area evaluation

	S048-1	S048-2
$\frac{I^{XPS}_{Bi}}{I^{XPS}_{Cu}}$	0.095 ± 0.01	0.115 ± 0.01
τ_{XPS}	0.75 ± 0.06	0.87 ± 0.06

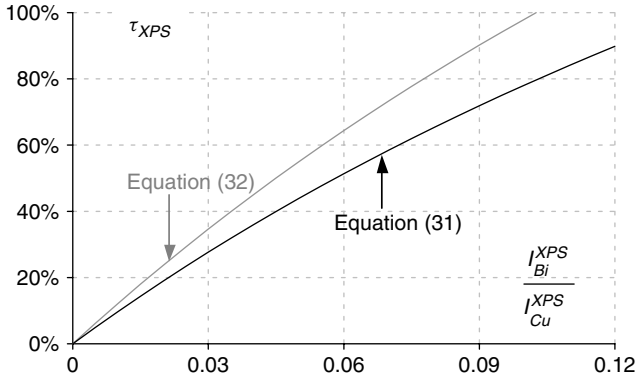

Figure 7. Graphical evolution of τ_{XPS} as a function of $\frac{I^{XPS}_{Bi}}{I^{XPS}_{Cu}}$ depending on the inelastic mean free path evaluation: black curve is obtained with Eqn (31) and grey curve with Eqn (32).

It leads to significant deviations from our τ_{XPS} calculations (Fig. 7). In the case of S048-1, 0.92 monolayer of bismuth is obtained with Eqn (32) instead of 0.75 monolayer with Eqn (31). Then, it appears that XPS quantification results depend strongly on the choice of the inelastic mean free path evaluation.

RBS quantification

Referred to as a nuclear analysis technique, the RBS is based on the measurement of the scattering yield of high-energy light ions, accelerated in the MeV domain. RBS enables absolute determination of elemental concentrations, since the

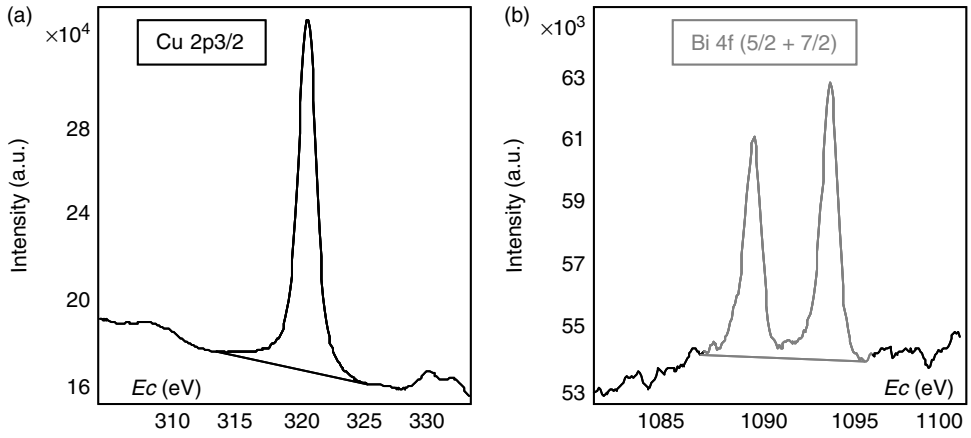

Figure 6. Direct XPS spectra from the surface for sample 1 (*in situ* fractured S048-1 specimen): (a) Cu2p$^{3/2}$ peak and (b) Bi4f$^{5/2}$ and Bi4f$^{7/2}$ peaks.

scattering cross-sections depend only on nuclear parameters. Thus, as a first approximation, data derived from RBS spectra are independent of the chemical environment of the elements and do not require acquisitions on reference or standard samples.

Data analysis

The present experiments have been conducted with a 2.5-MeV $^4He^+$ beam and a particle detector placed at 170° from the beam axis (*cf* Figure 8). The usual treatment of RBS data is based on simulation programs such as SIMNRA code,[23] by adjustment of computed spectra on experimental ones. However, in the case of ultra-thin bismuth layers on copper substrate, the spectra are simple enough to be treated manually. The foreseen advantage of a manual procedure is an easy access to the values of the physical parameters involved, which enables an evaluation of precision and accuracy.

Considering a thin sample to be analysed, the corresponding number of backscattered particles detected for a given element may be expressed as follows:

$$I^{RBS} = \sigma(E, \Theta) \times \Omega \times Q \times N \times h \tag{33}$$

with:

- $\sigma(E, \Theta)$ is the scattering cross-section on the element at the energy E of the incident particles (supposed to be constant within the sample) and for the scattering angle Θ (defined by the position of the particle detector),
- Ω the solid angle spanned by the detector,
- Q the total number of incident particles,
- N the atomic density of the element in the sample and
- h the thickness of the slab.

Note that the $N \times h$ product is the number of target atoms in a unit of area and corresponds to the atomic (or mass) thickness of the slab, whatever its density. To be compared to AES and XPS results, this value will have to be converted in the bismuth monolayer fraction τ_{RBS} (*cf* Eqn (42) hereafter).

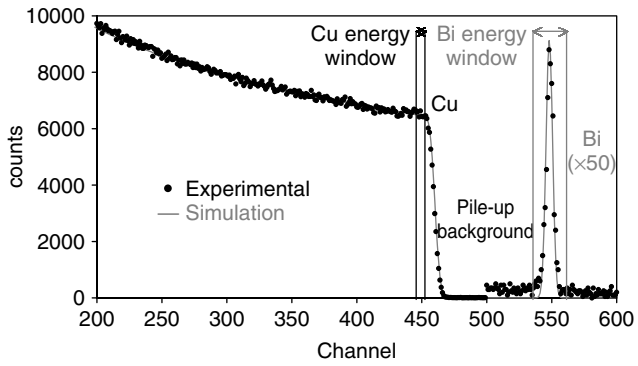

Figure 8. Experimental RBS spectrum of copper crystal surface covered with bismuth, obtained with 2.5-MeV 4He$^+$ beam and a detection angle of 170°. The energy Bi and Cu windows considered for quantification are indicated. A simulation of the data with the SIMNRA code is also plotted.

In the case of an ultra-thin bismuth layer on the top of a bulk copper sample, the bismuth appears in the spectrum as a single Gaussian peak, whereas the cooper produces the usual RBS step (*cf* Figure 8). The two signals are interference-free, except a very low smooth background under the bismuth peak due to pile-up from scattering on copper. The Eqn (33) can be directly applied to quantify the bismuth layer since the scattering occurs on the surface of the sample, exactly at the energy of the beam (2.5 MeV). The precision and accuracy on the determined bismuth content depend on each term of Eqn (33), as discussed below.

RBS parameters evaluation

The scattering cross-sections are accurately known. Basically, their energy and angular dependence follow Rutherford's model based on Coulombian interactions:

$$\sigma_R(E,\Theta) = 5.1837 \times 10^6 \left(\frac{Z_1 Z_2}{E}\right)^2 \times \frac{[(M_2^2 - M_1^2 \sin^2\Theta)^{1/2} + M_2 \cos\Theta]^2}{M_2 \sin^4\Theta (M_2^2 - M_1^2 \sin\Theta)^{1/2}} \tag{34}$$

where Z_1 and M_1 are the nuclear charge and the mass of the projectile, respectively, and Z_2 and M_2 those of target atom.

Experimental measurements indicate that actual cross-sections depart from Rutherford's. In the present case, these deviations are taken into account, but they are low. At low energy (<a few MeV), a partial screening of the nuclear charges by the electron shells occurs. A correction factor F has to be applied and:

$$\sigma = F \times \sigma_R \tag{35}$$

Several semiempirical expressions have been proposed to take into account the energy and angular dependence of the correction factor[24,25] but, for $\Theta > 90°$, all the models tend to the same value, depending only on the energy and on the target–projectile pair. For a 2.5-MeV $^4He^+$ beam on bismuth, the correction factor at 170° is lower than 1% and can be accurately determined.

Departures from Rutherford cross-sections may also occur from the presence of short-range nuclear forces. These forces become significant only for a very short distance between the projectile and the target nuclei, i.e. either for high-energy projectiles or light target atoms (limited Coulombian repulsion between target and projectile). At 170° for a 2.5-MeV $^4He^+$ beam, this deviation from Rutherford scattering no longer excess 4% for fluorine ($Z_2 = 9$) and is insignificant for bismuth ($Z_2 = 83$).

Another source of uncertainty is obviously the estimation of the yield of the bismuth backscattering from the bismuth peak. In our experimental conditions, the integral of the bismuth peak for a monolayer is typically 1000 counts. On the basis of a simple $\sqrt{N}/N$ estimator, the precision on the yield is in the order of ±3%. For ultra-thin bismuth layers, an additional error may come from pile-up background subtraction (*cf* Figure 8).

The last source of errors lies in the estimation of the product $\Omega \times Q$. Two methods may be applied:

- *Absolute determination of Q and* Ω: Since the beam intensity usually varies during the acquisition, the number of incident particles cannot be accurately deduced from beam time. A direct measurement of Q is made from the charge induced in the sample by the ions of the beam (each individual $^4He^+$ ion brings one elemental charge). Because the ion beam induces emission of secondary electrons, whose loss raises the positive charge of the sample, a 90-V positive bias is applied to the sample holder to collect them again. The typical accuracy of charge measurements is within 3–4%, sometimes higher (incomplete trapping of secondary electron produces systematic errors).

An estimation of the solid angle Ω can be set from the dimensions and the position of the detector holder, but the most accurate value should be deduced from an acquisition on a standard sample. However, as this latter measurement needs also charge measurement, the accuracy cannot be significantly better than 2%.

To improve the precision, a second method, based on internal standardization described below, has been preferred.

- *Use of copper as internal standard*: Equation (33) can be applied only when the scattering cross-section remains constant, that is to say, in the case of a thin layer. It remains valid when considering a thin slab of the copper substrate, which contributes to the spectrum by I_{Cu}^{RBS}. As bismuth and copper are detected simultaneously, the same $\Omega \times Q$ product applies. Then the bismuth film thickness h_{Bi} can be deduced from:

$$N_{Bi} \times h_{Bi} = \frac{I_{Bi}^{RBS}}{I_{Cu}^{RBS}} \times \frac{\sigma_{Cu}(E, \Theta)}{\sigma_{Bi}(E, \Theta)} \times N_{Cu} \times h_{Cu} \qquad (36)$$

Like for bismuth, the scattering cross-sections on copper are practically Rutherford, with a very low screening contribution (F) and no effect of short-range nuclear interactions. The ratio $\sigma_{Cu}(E, \Theta)/\sigma_{Bi}(E, \Theta)$ is then known accurately.

The issue for an accurate internal standardization is to link the yield of backscattering I_{Cu}^{RBS} to the proper quantity of copper analysed $N_{Cu} \times h_{Cu}$. Whereas for bismuth, the integral of the RBS peak, I_{Bi}^{RBS}, represents the whole film, for the copper I_{Cu}^{RBS} is related to a slab whose thickness depends on the stopping power of ^4He ions in copper. This slab contributes to the content of a few channels in the spectrum, which defines an energy window of width δe (*cf* Figure 8). δe comes from the longer path of the particles backscattered at the bottom of the slab since they have to go twice through the layer, before and after the backscattering event.

Introducing $[\varepsilon]$, the stopping cross-section factor of the particles of the beam, the depth scale is given by:

$$\delta e = [\varepsilon] \times N_{Cu} \times h_{Cu} \qquad (37)$$

which gives, combined with Eqn (34):

$$N_{Bi} \times h_{Bi} = \frac{I_{Bi}^{RBS}}{I_{Cu}^{RBS}} \times \frac{\sigma_{Cu}(E, \Theta)}{\sigma_{Bi}(E, \Theta)} \times \frac{\delta e}{[\varepsilon]} \qquad (38)$$

The energy loss of the particles of the beam in the sample varies with their energy. Then, $[\varepsilon]$ is not a primary parameter since it combines both inward and outward paths, before and after the scattering, respectively. It can be computed in any case, but the simplest expression comes in the case of a surface slab, when:

$$\delta e = K \times E_0 - E_1 \qquad (39)$$

where E_0 is the energy of the particles of the beam, K the kinematic factor and E_1 the energy of the detected particles coming from the depth h_{Cu}. It comes from Eqns (35) and (37):

$$[\varepsilon] = \left(K \times \varepsilon_{in} + \frac{1}{\cos\theta} \times \varepsilon_{out} \right) \qquad (40)$$

with θ being the angle between the beam and the backscattered particles (with the sample normal to the beam). ε_{in} and ε_{out} are the stopping cross sections along the inward and outward paths, practically constant for a thin layer. The values of ε_{in} and ε_{out} are taken for energies E_0 and KE_0, respectively.

RBS results

The example of quantification given below is based on the spectrum of Fig. 8 from which values of I_{Bi}^{RBS}, I_{Cu}^{RBS} and δe are directly extracted. I_{Bi}^{RBS} is the net area of the bismuth peak (1158 counts), pile-up background deducted. I_{Cu}^{RBS} is the content of an energy window open in the surface region of the copper step (32 341 counts integrated in five channels). δe is the energy width of this window deduced from the energy calibration of the particle detector (5 × 4.22 keV/channel).

The geometry of detection defines a scattering mean angle Θ of 170°. At the energy of the incident ^4He beam (2.5 MeV), the corresponding cross-sections σ_{Cu}(2.5,170) and σ_{Bi}(2.5,170) are 700 mb/sr and 5712 mb/sr, respectively. The kinematic factor K for $^4He^+$ scattering on copper is equal to 0.778 at 170° and the angle θ is 10°.

The stopping cross-sections of light ions are accurately known for medium and heavy target elements. Although an overall increase of ε on the mass of the target element may be easily computed, departures from the mean law exist. A decrease in the stopping cross section occurs when d-shell electrons are added in the sequence of transition elements, such as from Ca to Cu or from Nb to Ag. In this case, the electron density near the atom increases enough to reduce the average electron density seen by an energetic particle traversing the material. The copper corresponds to a minimum with ε values lowered by typically 10% below a mean law value.

To benefit from accurate values, stopping cross-sections in copper have been computed with the Ziegler's SRIM2003 code.[26,27] ε_{in} is found to be 61.5 eV/10^{15} at cm^{-2} for 2.5 MeV ^4He and ε_{out} to be 66.6 eV/10^{15} at cm^{-2} for 1.946 MeV ^4He (KE_0).

From the injection of these values in Eqn (36), it becomes:

$$N_{Bi} \times h_{Bi} = 0.81 \times 10^{15} \text{ at cm}^{-2} \qquad (41)$$

The bismuth monolayer fraction τ_{RBS} can be related to this value with the help of the atomic thickness of a bismuth monolayer n_{Bi}:

$$N_{Bi} \times h_{Bi} = \tau_{RBS} \times n_{Bi} \qquad (42)$$

Taking into account the evaluation of the thickness of a monolayer presented in the AES section (cube root of the atomic volume), n_{Bi} is evaluated as 0.93×10^{15} at cm^{-2} (=9.3 at nm^{-2}). The thickness of the bismuth layer of Fig. 8 is then estimated to be:

$$\tau_{RBS} = \frac{N_{Bi} \times h_{Bi}}{n_{Bi}} \approx 0.87 \; monolayer \qquad (43)$$

The results for two samples, S048-1 and S137-1 are reported in Table 3.

The uncertainties on these thickness may be easily estimated from Eqn (36). Errors on I_{Bi}^{RBS} and I_{Cu}^{RBS} are only statistical fluctuations. Taking the square root of the value as an estimator, typical errors are ±0.5% for I_{Cu}^{RBS} and ±3% for I_{Bi}^{RBS}. The cross-sections σ_{Cu}(2.5,170) and σ_{Bi}(2.5,170) are accurately known, better than ±1%, since the correction factor from Rutherford cross-sections due to screening effects is very close to 1 in our experimental conditions. The accuracy of δe depends on the quality of the energy calibration of the particle detector, typically ±0.5% provided a broad range of energy positions of RBS steps have been checked (target elements of different mass).

The main source of inaccuracy is the estimation of the stopping cross-sections. Ziegler's SRIM code calculations are based on a quantum mechanical treatment of ion–atom collisions, validated on experimental data. ^{1}H and ^{4}He, as projectiles, have been by far the most studied, and the corresponding models for their respective stopping cross-sections produce values with a good accuracy, below 4% in our present energy range.

In conclusion, the relative precision of RBS bismuth thickness measurements depends on statistical fluctuations on the bismuth and copper signals, typically ±3.5%, whereas the accuracy is dominated by stopping-power estimation ±4%. The overall accuracy may be then estimated to ±10%.

Table 3. Experimental fractions of bismuth monolayer τ_{RBS} obtained by RBS analyses

	S048-1	S137-1
τ_{RBS}	0.87 ± 0.08	0.87 ± 0.08

DISCUSSION

Validation of physical assumptions

The purpose stated in the introduction was to perform comparative measurements using complementary methods (XPS, AES and RBS) in order to get a reliable picture of the quantity of bismuth present in a copper grain boundary after a contact between the solid copper bicrystal and liquid bismuth. To achieve this goal, two main assumptions had to be stated, namely: homogeneous bismuth distribution on the fracture surfaces and equirepartition.

The first assumption that a homogeneous layer of bismuth is present on the copper substrate is critical for XPS because of a very large (3 mm) spot size of a twin anode used. Figure 9 shows a series of AES analyses made on different locations of a fracture surface. It clearly indicates that bismuth coverage is almost constant on the whole specimen surface, confirming our assumption.

The second assumption concerns the equirepartition of bismuth after the fracture: it is needed to get valuable information about the initial intergranular bismuth presence before the fracture. Figure 10 shows two RBS analyses made on two opposite sides of a fracture surface. It confirms that bismuth is equally distributed on both sides of the fracture surface. This is in agreement with a previous study based on AES analyses made on copper–bismuth alloys fracture surfaces where the bismuth concentration was similar on the two matching fracture surfaces.[28]

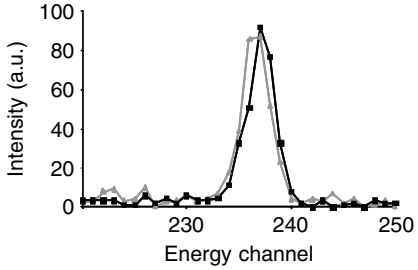

Figure 10. RBS experimental bismuth peaks obtained on two sides of the fracture surface of the same sample: the same quantity of bismuth is present on both of them (intensities have been normalised with respect to copper signal in order to get a relevant comparison).

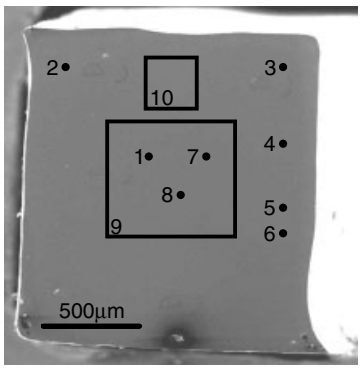

Position	τ_{AES}	*Position*	τ_{AES}
1	*0.78*	*6*	*0.81*
2	*0.82*	*7*	*0.83*
3	*0.76*	*8*	*0.81*
4	*0.78*	*9*	*0.85*
5	*0.82*	*10*	*0.84*

Figure 9. SEM picture of the S048-1 fracture surface: points are AES spot analyses (1–8) whereas squares are AES scan analyses (9–10). Bismuth coverage is given (in fraction of monolayer) for each analysis according to the procedure described in a previous paragraph and using Eqn (17): the average τ_{AES} value is 0.81 for this example.

Validation of the mathematical models

Instead of using methods based on a discrete summation for AES and XPS quantifications, continuous summation can also be made. Concerning AES, this does not lead to any changes in the results, as the final equations relating bismuth-to-copper experimental intensity ratio to bismuth coverage are strictly the same (as shown in Appendix). On another hand, XPS results can vary with the choice of the summation method. With the discrete summation, Eqns (23) and (31) have been obtained. On the other hand, a continuous summation can also be used. Equations become:

$$I_{Bi}^{XPS} = \tau_{XPS} K_{XPS} N_{Bi} \sigma_{Bi} T_{Bi} \times \int_0^{d_{Bi}} \exp\left(\frac{-z}{\lambda_{Bi}^{Bi} \cos\theta}\right).\mathrm{d}z$$
$$= \tau_{XPS} K_{XPS} N_{Bi} \sigma_{Bi} T_{Bi} [1 - k_{Bi}^{Bi}] \lambda_{Bi}^{Bi} \cos\theta \quad (44)$$

and

$$I_{Cu}^{XPS} = K_{XPS} N_{Cu} \sigma_{Cu} T_{Cu} [(1 - \tau_{XPS}) + \tau_{XPS} k_{Cu}^{Bi}]$$
$$\times \int_0^{+\infty} \exp\left(\frac{-z}{\lambda_{Cu}^{Cu} \cos\theta}\right).\mathrm{d}z$$
$$= K_{XPS} N_{Cu} \sigma_{Cu} T_{Cu} [(1 - \tau_{XPS}) + \tau_{XPS} k_{Cu}^{Bi}] \lambda_{Cu}^{Cu} \cos\theta \quad (45)$$

Term N is the number of atoms per unit volume estimated using the following relationship: $N = \frac{\rho \times N_{avogadro}}{M}$. The followings values were used:

$N_{Bi} \approx 2.82 \times 10^{28}$ atoms m^{-3} and $N_{Cu} \approx 8.43 \times 10^{28}$ atoms m^{-3}.

The inelastic mean free path λ_{Bi}^{Bi} was then calculated:

$\lambda_{Bi}^{Bi} \approx 2.57$ nm (7.8 monolayers) for both Bi $4f^{5/2}$ and $4f^{7/2}$ kinetic energies

In this case, the fraction of bismuth monolayer τ_{XPS} present on the fracture sample can be related to the experimental bismuth-to-copper ratio with the following equation:

$$\tau_{XPS} = \frac{\frac{I_{Bi}^{XPS}}{I_{Cu}^{XPS}}}{\frac{N_{Bi}\lambda_{Bi}^{Bi}[\sigma_{Bi-4f^{7/2}} + \sigma_{Bi-4f^{5/2}}]T_{Bi}}{N_{Cu}\lambda_{Cu}^{Cu}\sigma_{Cu-2p^{3/2}}T_{Cu}}[1 - k_{Bi}^{Bi}] + \frac{I_{Bi}^{XPS}}{I_{Cu}^{XPS}}[1 - k_{Cu}^{Bi}]} \quad (46)$$

Using the previously described parameters calculation, the following relationship appears:

$$\tau_{XPS} \approx \frac{\frac{I_{Bi}^{XPS}}{I_{Cu}^{XPS}}}{0.09 + 0.28 \times \frac{I_{Bi}^{XPS}}{I_{Cu}^{XPS}}} \quad (47)$$

Equation (43) is rather similar to Eqn (31) and that proves the equivalence between the two approaches: both discrete and continuous summations give consistent results with each others.

Inelastic mean free paths versus effective attenuation lengths

The reasons that led us to use IMFP instead of effective attenuation lengths[29] (EAL) in both AES and XPS quantifications are the following:

- we wanted to get a direct comparison between our studies made on the copper/bismuth system and previous studies made with equivalent procedures on the nickel/bismuth system where the authors had used the IMFP in their AES quantification,[9]
- taking IMFP instead of EAL in the quantifications leads clearly to an overestimation of the bismuth coverage as the EAL are usually about 10 to 20% less than the IMFP; nevertheless, this 'intentional' overestimation makes us feel even more confident on our conclusions about the absence of grain-boundary wetting (see the following text).

Coherency of the results

AES measurements have shown the presence of $82 \pm 18\%$ of bismuth monolayer on the analysed fracture surfaces. On another hand, XPS measurements have shown the presence of $81 \pm 12\%$ of bismuth monolayer on the same surfaces, the uncertainty being due to the spectra exploitation rather than to the physical parameters calculations. RBS measurements have shown the presence of $87 \pm 8\%$ of bismuth monolayer on the same surfaces. As a conclusion, all results are therefore consistent with each other, with a significantly larger deviation for AES measurements.

Our results are very close to those obtained by AES quantification of bismuth grain boundary segregation into copper.[30–32] As a matter of fact, our study shows that the contact between solid bicrystalline copper and liquid bismuth leads to the presence of about $2 \times 0.8 = 1.6$ monolayers of bismuth in the copper grain boundary. This is in fair agreement with the upper value of two monolayers found after grain boundary segregation. So, this would indicate that even with a contact between solid copper and liquid bismuth (saturated with copper), bismuth intergranular presence is controlled by the same thermodynamic equilibrium as that of intergranular segregation: namely, the number of sites of the grain boundary energetically in favour of bismuth presence.

Implications on LME phenomenon

These results mean also that we are far from a liquid bismuth invasion of the copper grain boundary. Such a conclusion is very important as a number of models proposed to describe LME are based on the grain boundary wetting that leads to the replacement of the initial grain boundary by a nanometer-thick intergranular liquid phase. In our case, Cu/Bi system after heat-treatment at 500 °C for 137 hours, we did not observe such a phenomenon. This is in apparent contradiction with earlier results obtained using XPS for the same Cu/Bi system where several monolayers of bismuth were thought to exist in a copper grain boundary[6] (heat treatment: 8 h at 600 °C). Yet, Joseph[33] made complementary AES analyses on a $2.0 \times 3.5\ \mathrm{mm}^2$ bicrystalline fracture surface (heat treatment: 2 h at 600 °C) and found an homogeneous bismuth coverage of about 93% of the monolayer, which is in reasonable agreement with our present results.

This work strongly suggests that intergranular diffusion can be the mechanism responsible for bismuth grain boundary penetration into copper. Additional tests have

been performed in order to get information on the kinetics of this penetration. As this kinetics appears to be parabolic,[15,34] it strengthens the idea that intergranular diffusion of bismuth in copper is the mechanism controlling the liquid-bismuth induced intergranular embrittlement of copper.

CONCLUSIONS

Intergranular embrittlement of bicrystalline copper by liquid bismuth has been achieved at 500 °C using condensation of bismuth vapour on copper in sealed silica tubes without any applied stress (durations: 48 and 137 h). The resulting room temperature brittleness allowed *in situ* fractures for XPS and AES analyses as well as further *ex situ* RBS analyses.

AES, XPS and RBS measurements are in excellent agreement, showing the presence of about 1.6 to 1.7 monolayers of bismuth in the copper grain boundary: $2 \times 0.82 \approx 1.6$ monolayers according to AES analyses, $2 \times 0.81 \approx 1.6$ monolayers according to XPS analyses and $2 \times 0.87 \approx 1.7$ monolayers according to RBS analyses.

The quantification models were based on two assumptions that were both verified in this study. AES quantification allowed to validate the assumption of a homogeneous repartition of bismuth. On another hand, the equirepartition of bismuth into both sides of the fracture surfaces was verified using RBS measurements.

These results clearly indicate that the contact between copper bicrystal and liquid bismuth does not produce any grain-boundary wetting at 500 °C. As a matter of fact, the bismuth coverages obtained in this study are very close to those obtained in the same system for grain boundary segregation.

Acknowledgements

The authors wish to thank G. Santarini and A. Terlain (both from the French Atomic energy Commission) for fruitful discussions as well as the crew of the nuclear microprobe of the Laboratoire Pierre SUE, especially L. Daudin, H. Khodja and J.P. Gallien.

APPENDIX

When trying to quantify bismuth presence on a copper substrate, two different approaches can be used. Both introduce the assumption that bismuth coverage is present as a fraction of monolayer τ_{AES}. First, using a discrete summation (monolayer by monolayer), the AES bismuth to copper intensity ratio can be related to τ_{AES} with:

$$\frac{I_{Bi}^{AES}}{I_{Cu}^{AES}} = \frac{I_{Bi}^{0} R_{Bi}^{Cu}}{I_{Cu}^{0} R_{Bi}^{Bi}} \frac{1 - k_p^{Bi} k_{Bi}^{Bi}}{\dfrac{(1-\tau_{AES})}{\tau_{AES}} + k_p^{Bi} k_{Cu}^{Bi}} \tag{48}$$

(see the body of the article for more details)

Second, using a continuous summation, with the same notations presented for the previous approach and introducing N: number of atoms per unit volume and α (parameter that includes, like β, the ionisation cross section, the deexcitation probability and the analyser transmission function), the following equations are obtained:

$$I_{Bi}^{AES} = \tau_{AES} K_A \alpha_{Bi} N_{Bi} R_{Bi}^{Cu} \int_0^{d_{Bi}} \exp\left(\frac{-z}{\lambda_p^{Bi} \cos\varphi}\right) \times \exp\left(\frac{-z}{\lambda_{Bi}^{Bi} \cos\theta}\right) .\mathrm{dz}$$

$$= \tau_{AES} K_A \alpha_{Bi} N_{Bi} R_{Bi}^{Cu} \frac{[1 - k_p^{Bi} k_{Bi}^{Bi}]}{\left[\dfrac{1}{\lambda_p^{Bi} \cos\varphi} + \dfrac{1}{\lambda_{Bi}^{Bi} \cos\theta}\right]} \tag{49}$$

$$I_{Cu}^{AES} = K_A \alpha_{Cu} N_{Cu} R_{Cu}^{Cu} [\tau_{AES} k_p^{Bi} k_{Cu}^{Bi} + (1 - \tau_{AES})] \times \int_0^{+\infty} \exp\left(\frac{-z}{\lambda_p^{Cu} \cos\varphi}\right) \exp\left(\frac{-z}{\lambda_{Cu}^{Cu} \cos\theta}\right) .\mathrm{dz}$$

$$= \tau_{AES} K_A \alpha_{Cu} N_{Cu} R_{Cu}^{Cu} \frac{\left[\dfrac{(1-\tau_{AES})}{\tau_{AES}} + k_p^{Bi} k_{Cu}^{Bi}\right]}{\left[\dfrac{1}{\lambda_p^{Cu} \cos\varphi} + \dfrac{1}{\lambda_{Cu}^{Cu} \cos\theta}\right]} \tag{50}$$

$$I_{Bi}^{0} = K_A^0 \alpha_{Bi} N_{Bi} R_{Bi}^{Bi} \int_0^{+\infty} \exp\left(\frac{-z}{\lambda_p^{Bi} \cos\varphi}\right) \exp\left(\frac{-z}{\lambda_{Bi}^{Bi} \cos\theta}\right) .\mathrm{dz}$$

$$= \frac{K_A^0 \alpha_{Bi} N_{Bi} R_{Bi}^{Bi}}{\left[\dfrac{1}{\lambda_p^{Bi} \cos\varphi} + \dfrac{1}{\lambda_{Bi}^{Bi} \cos\theta}\right]} \tag{51}$$

and

$$I_{Cu}^{0} = K_A^0 \alpha_{Cu} N_{Cu} R_{Cu}^{Cu} \int_0^{+\infty} \exp\left(\frac{-z}{\lambda_p^{Cu} \cos\varphi}\right) \exp\left(\frac{-z}{\lambda_{Cu}^{Cu} \cos\theta}\right) \mathrm{dz}$$

$$= \frac{K_A^0 \alpha_{Cu} N_{Cu} R_{Cu}^{Cu}}{\left[\dfrac{1}{\lambda_p^{Cu} \cos\varphi} + \dfrac{1}{\lambda_{Cu}^{Cu} \cos\theta}\right]} \tag{52}$$

and thus:

$$\frac{I_{Bi}^{AES}}{I_{Cu}^{AES}} = \frac{I_{Bi}^{0} R_{Bi}^{Cu}}{I_{Cu}^{0} R_{Bi}^{Bi}} \frac{1 - k_p^{Bi} k_{Bi}^{Bi}}{\dfrac{(1-\tau_{AES})}{\tau_{AES}} + k_p^{Bi} k_{Cu}^{Bi}}$$

that is, again, Eqn (48).

It can appear useful to relate together the two parameters α and β. Comparing the equations obtained for pure elements according to both the discrete and the continuous summations and assuming $n_A = d_A \times N_A$, it comes: $\alpha_A = \dfrac{\beta_A \left[\frac{d_A}{\lambda_p^A \cos\varphi} + \frac{d_A}{\lambda_A^A \cos\theta}\right]}{1 - k_p^A k_A^A}$. It can be easily shown that, with d_A decreasing to 0, $\alpha_A = \beta_A$.

REFERENCES

1. Bauer GS, Salvatores M, Heusener G. *J. Nucl. Mater.* 2001; **296**: 17.
2. Bauer GS, Dai Y, Maloy S, Mansur LK, Ullmaier H. *J. Nucl. Mater.* 2001; **296**: 321.
3. Kikuchi K, Sasa T, Mukugi K, Kai T, Ouchi N, Ioka I. *J. Nucl. Mater.* 2001; **296**: 34.
4. Fernandes PJL, Jones DRH. *Int. Mater. Rev.* 1997; **42**: 251.
5. Joseph B, Barbier F, Aucouturier M. *Eur. Phys. J-Appl. Phys.* 1999; **5**: 19.
6. Joseph B, Barbier F, Dagoury G, Aucouturier M. *Scripta Mater.* 1998; **39**: 775.
7. Joseph B, Barbier F, Aucouturier M. *Mater. Sci. Forum.* 1999; **735**: 294.
8. Marié N, Wolski K, Biscondi M. *J. Nucl. Mater.* 2001; **296**: 282.
9. Wolski K, Marié N, Biscondi M. *Surf. Interface Anal.* 2001; **31**: 280.

10. Joseph B, Barbier F, Aucouturier M. *J. Phys. Iv* 1999; **9**: 235.
11. Fraczkiewicz A, Biscondi M. *J. Phys.* 1985; **46**: 497.
12. Fraczkiewicz A. *Ségrégation d'équilibre du bismuth aux joints de flexion pure dans le cuivre: étude expérimentale et simulation par ordinateur*, Ecole des Mines de Saint-Etienne, 1986.
13. Marié N. *Etude de la pénétration intergranulaire fragilisante du bismuth liquide dans le nickel solide à 700 °C*, Université Jean Monnet de Saint-Etienne: Saint-Etienne (France), 2003.
14. Chang LS. *Untersuchungen zur Thermodynamik und Kinetic der Korngrenzensegregation von Bi in Cu*. Universität Stuttgart: Stuttgart (Germany), 1998.
15. Laporte V, Wolski K. to be submitted to Scripta Materialia.
16. Shimizu R. *Jpn. J. Appl. Phys.* 1983; **22**: 1631.
17. Tanuma S, Powell CJ, Penn DR. *Surf. Interface Anal.* 1991; **17**: 911.
18. Tanuma S, Powell CJ, Penn DR. *Surf. Interface Anal.* 1993; **20**: 77.
19. Tanuma S, Powell CJ, Penn DR. *Surf. Interface Anal.* 1994; **21**: 165.
20. Seah MP. *Surf. Interface Anal.* 1990; **1**: 201.
21. Jablonski A. *Surf. Sci.* 2002; **499**: 19.
22. Grimblot J. *L'analyse de Surface des Solides par Spectroscopies Électroniques et Ioniques*. Masson: Paris, 1995.
23. Mayer M. *SIMNRA User's Guide*. Max-Planck-Institüt für Plasmaphysic: Garching (Germany), 1997.
24. L'Ecuyer J, Davies JA, Matsunami N. *Nucl. Instrum. Methods Phys. Res. Sect. B-Beam Interact. Mater. Atoms* 1979; **160**: 337.
25. Andersen HH, Besenbacher F, Loftager P, Möller W. *Phys. Rev. A* 1980; **21**: 1891.
26. Ziegler JF, Biersack JP, Littmark U. *The Stopping and Range of Ions in Solids*, vol. 1. Pergamon Press: New-York, 1984.
27. Ziegler JF. www.srim.org. 2004.
28. Powell BD, Mykura H. *Acta Metall.* 1973; **21**: 1151.
29. Powell CJ, Jablonski A. *Surf. Interface Anal.* 2002; **33**: 211.
30. Chang LS, Rabkin E, Straumal BB, Baretzky B, Gust W. *Acta Mater.* 1999; **47**: 4041.
31. Chang LS, Rabkin E, Straumal BB, Lejcek P, Hofmann S, Gust W. *Scripta Mater.* 1997; **37**: 729.
32. Chang LS, Rabkin E, Hofmann S, Gust W. *Acta Mater.* 1999; **47**: 2951.
33. Joseph B. *Fragilisation du Cuivre Par le Bismuth Liquide: Étude Cinétique et Mécanisme*. Université de Paris XI: Orsay, 1998.
34. Laporte V, Wolski K, Berger P, Terlain A, Santarini G. *Defect Diffus. Forum* 2005; **683**: 237.